

MODELLING OF CROSSFLOW-INDUCED TRANSITION BASED ON LOCAL VARIABLES

Christoph Müller¹, Florian Herbst¹

¹Leibniz Universität Hannover
Institute of Turbomachinery and Fluid Dynamics
Appelstraße 9, D-30167, Hannover, Germany
e-mail: mueller@tfd.uni-hannover.de

Key words: CFD, transition, boundary layer, crossflow

Abstract. Crossflow instabilities on swept wings lead to an accelerated transition and therefore greatly increased profile losses. Modern CFD codes therefore must have the capability to predict crossflow-induced boundary layer transition. For this purpose, an additional mode of destabilization was added into the framework of the $\gamma - Re_\theta$ model. The Reynolds number Re_H based on the local helicity was found to be a key parameter in order to detect crossflows within boundary layers. The model formulation is in accordance with the baseline $\gamma - Re_\theta$ model, since only local quantities are used. Therefore the model can be applied on complex three-dimensional geometries. The model was calibrated on two infinite swept wing test cases, where the Reynolds number and the sweep angle were varied, respectively. A good match to experimental data was achieved. For the purpose of validation a 1:6 spheroid was taken into account. Although the prediction is lacking on this test case, a correct detection of crossflows can be observed.

1 INTRODUCTION

Predicting transition in boundary layers is fundamental when it comes to drag reduction, as turbulent boundary layers cause significantly higher shear stresses. The transition of a laminar boundary layer on swept wings can be initiated by four fundamental modes. These are based on the high turbulence near the wing root, the growth of primary instabilities due to Tollmien-Schlichting waves, centrifugal instabilities resulting in the formation of Görtler vortices or crossflow instabilities [1, 2]. These modes can promote or delay each other. This paper is focused on the development of crossflow instabilities.

Crossflow instabilities can occur on swept airfoils under the presence of a pressure gradient. Under these conditions the pressure gradient vector close to the profile leading edge is not on the same plane as the streamlines of a two-dimensional profile flow, but is rotated by the sweep angle of the profile. Therefore the streamlines around the swept profile

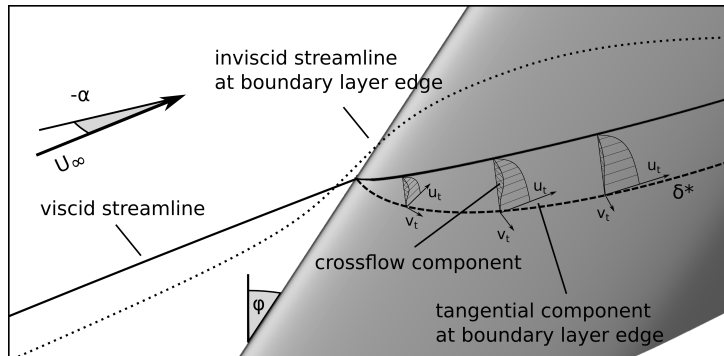


Figure 1: Sketch of a crossflow profile on a swept wing

are three-dimensionally deflected. This leads to inertial and pressure forces maintaining equilibrium. Within the boundary layer viscous effects reduce velocity, which results in lower pressure and inertial forces. Consequently, streamlines within the boundary layer are less curved.

This change in the streamline curvature induces high velocity gradients, resulting in the development of secondary flows. The induced boundary layer profile is highly swept and includes an inflection point within the crossflow component (Fig. 1). This causes an inflectional instability accelerating transition. As discussed by Arnal and Casalis [3] the crossflow component of the velocity profile can reach about 5 – 10% of the free stream velocity in the accelerated areas of the profile leading edge. This causes strong crossflows resulting in stationary waves. These waves are observed to be directly related to the presence of primary crossflow instabilities [4, 5]. Traveling wave disturbances indicate the final stage of transition. These secondary instabilities are resulting from ring-like vortices that are aligned around the primary vortex [5]. They contribute significantly to the final stage of the transition process.

When the three-dimensional boundary layer is decelerated further downstream, the curvature of the streamline at the boundary layer edge changes. The intensity of crossflow vortices drops immediately. If the transition to turbulence has not taken place upstream of this point, present instabilities can trigger the development of traveling waves (Tollmien-Schlichting waves) and thereby initiate natural transition [5, 3].

Deyhle and Bippes [6] investigated the influence of turbulence on the development of crossflow instabilities. As they pointed out, a rise in the level of turbulence can lead to a suppressed transition while $Tu < 0.2\%$, in their case. Higher levels of turbulence ($Tu > 0.2\%$), however, led to an accelerated transition, as traveling waves increase with turbulence, suppressing the stationary waves [7].

As the level of turbulence rises above $Tu = 0.2\%$, earlier steps of transition are bypassed and thus natural transition is the dominant phenomenon.

As wall shear stresses of turbulent boundary layers increase up to a factor of four, in comparison to laminar boundary layers, the resultant pressure losses are significantly

higher. Therefore, correctly predicting laminar-turbulent transition is an invaluable tool for aerodynamic engineers. A wide variety of approaches to improve the prediction accuracy of CFD solvers have been made in the past few years.

A widely used method in applied aerodynamics is the e^N -method which is based on linear stability analysis [3, 2, 8]. The e^N -method is basically designed for two-dimensional boundary layers but it can be extended to three-dimensional boundary layers, however it still exhibits some deficiencies [3]. A major disadvantage of this method is that the N -factor, which is responsible for a critical amplification of linear disturbances, has to be fit to each test case. Additionally, the application of the e^N -method into a RANS code is complicated by the fact that the boundary layer code has to be solved parallel to the free stream flow field. Integral boundary layer quantities have to be exchanged between both applications.

A new approach had been made in terms of the $\gamma - Re_\theta - Re_{\delta 2t}$ -model by Seyfert and Krumbein [9]. In their work, the $\gamma - Re_\theta$ -model by Langtry and Menter [10] had been extended to predict crossflow-induced transition. The baseline $\gamma - Re_\theta$ -model uses a locally defined streamwise Reynolds number Re_V . Analogous to this formulation, Seyfert and Krumbein used a Reynolds number $Re_{V,y}$ based on the crossflow velocity component perpendicular to the free stream. As this value reaches a critical level, transition is initiated. The definition of this critical value is based on the well-known $C1$ -criterion including a locally evaluated Falkner-Scan-Cooke solution. The resulting model shows promising results with the investigated NLF(2)-0415 profile as well as the ONERA 'D' profile. Nevertheless, this model is dependent on the profiles sweep angle, which has to be given as a boundary condition. Therefore a reduced applicability on complex three-dimensional geometries is expected by the author.

Based on the $\gamma - Re_\theta$ -model a different approach had been made earlier by Watanabe et al. [11]. It uses the streamline curvature parameter C_K defined by Kohama and Davis [12], and compares this locally defined parameter with a critical value $C_{threshold}$. As this value is exceeded transition is initiated very abruptly by the use of the separation induced transition mode. This method is strictly based on local quantities and therefore applicable on complex geometries but it lacks in the ability to cover flow historical effects. As described by Arnal and Casalis [3], crossflow instabilities do not need to be present during the whole transition process but can also initiate natural transition. Therefore, interacting with the natural transition mode, as done by Seyfert and Krumbein, allows for a better consideration of physical flow effects.

2 NUMERICAL METHOD

In the present work modelling crossflow-induced transition is based on $\gamma - Re_\theta$ -transition model by Langtry and Menter [10], as it has been used by Watanabe et al. [11] and Seyfert and Krumbein [9]. The $\gamma - Re_\theta$ -model follows the basic idea that only local quantities are used in order to predict transition. As a result it is applicable on unstructured computational grids and complex three-dimensional geometries such as the spheroid investigated

by Kreplin et al. [13] or the segmental swept wing introduced by Petzold and Radespiel [8]. For this purpose, two transport equations for $\tilde{Re}_{\theta t}$ and γ are used to cover flow historical effects.

$\tilde{Re}_{\theta t}$ is linked to the Reynolds number based on the momentum loss thickness deduced from the correlations by Abu-Ghannam and Shaw [14]. Therefore, this mode of transition covers natural transition, and also bypass-induced transition for higher levels of turbulence. Whenever the locally defined vorticity Reynolds number

$$Re_V = \frac{\rho y^2}{\mu} S, \quad (1)$$

exceeds a critical Reynolds number based on $\tilde{Re}_{\theta t}$, transition is initiated. In this case ρ is the density, y is the distance from the nearest wall, μ is the dynamic viscosity and S is the shear strain rate. Transition is initiated by increasing the second transport quantity γ , intermittency. This is representative of the production of turbulent kinetic energy. The separation induced transition mode is realized by increasing γ directly.

The $\gamma - Re_{\theta}$ -model is implemented into the RANS-solver TRACE. TRACE was developed by the DLR Cologne in cooperation with MTU Aero Engines AG as an industrial partner [15, 16]. Therefore TRACE was validated on a broad variety of turbomachinery and generic test cases. TRACE provides a spatial discretization for convective fluxes with a 2nd order accuracy based on an upwind scheme by Roe [17]. Diffusive fluxes are discretized by a 2nd order central scheme. The turbulence model used for the calibration is the $k - \omega$ -model by Wilcox [18] combined with the stagnation point anomaly fix by Kato and Launder [19].

3 THE SET OF TESTCASES

For the model calibration, two profiles were taken into account. The first is the ONERA 'D' profile, which was investigated by Schmitt and Manie [20]. It is a section from the ONERA M6 wing and it is used for calibration on one Reynolds number $Re = 1.0 \cdot 10^6$ under varying sweep angles from $\varphi = 40^\circ, 50^\circ$ to 60° . The second test case is the NLF(2)-0415 profile which was experimentally investigated by Dagenhart and Saric [2]. On this test case the sweep angle maintained $\varphi = 45^\circ$ and the calibration was conducted for a Reynolds number from $Re = 1.92 \cdot 10^6$ to $Re = 3.27 \cdot 10^6$.

The extend of the farfield boundary condition was set to 20 times the profile chord length in diameter. As the sweep angle of the ONERA 'D' profile is varied, a single grid with a $\varphi = 0^\circ$ sweep angle was generated and the boundary conditions were used to change φ . Therefore, spanwise boundary conditions are set to periodic. The NLF(2)-0415 grid includes the $\varphi = 45^\circ$ sweep angle and the Reynolds number is varied by the free stream velocity. In order to minimize computational cost, the spanwise extent h of the computational grids was minimized so that $\frac{h}{l_{\text{ONERA 'D'}}} = 0.75$ for the ONERA 'D' profile and $\frac{h}{l_{\text{NLF(2)-0415}}} = 2.88$ for the NLF(2)-0415 profile, respectively. A study was performed

Table 1: List of boundary conditions

Tu_∞ in %	L_{Tu} in m	Ma_∞	Re	φ_∞ in deg.	α_∞ in deg.	$x/l_{t,Exp.}$
ONERA 'D'						
1.0	$1.3 \cdot 10^{-4}$	0.224	$1.0 \cdot 10^6$	40	-7.72	0.92
1.0	$1.55 \cdot 10^{-4}$	0.224	$1.0 \cdot 10^6$	50	-9.187	0.44
1.0	$1.99 \cdot 10^{-4}$	0.224	$1.0 \cdot 10^6$	60	-11.74	0.25
NLF(2)-0415						
1.0	$0.6 \cdot 10^{-4}$	0.123	$1.92 \cdot 10^6$	45	-4	0.78
1.0	$0.6 \cdot 10^{-4}$	0.140	$2.19 \cdot 10^6$	45	-4	0.73
1.0	$0.6 \cdot 10^{-4}$	0.151	$2.37 \cdot 10^6$	45	-4	0.58
1.0	$0.6 \cdot 10^{-4}$	0.174	$2.73 \cdot 10^6$	45	-4	0.45
1.0	$0.6 \cdot 10^{-4}$	0.209	$3.27 \cdot 10^6$	45	-4	0.33

to ensure that no impact on the results could be observed. All boundary conditions are summarized in Tab. 1.

4 GRID CONVERGENCE INDEX

Numerical simulations are subjected to different types of errors [21]. One of these is the discretization error, which is dependent on the computational mesh. Particularly in terms of numerical model calibrations, an estimation of the underlying discretization error is required. The procedure of a Grid Convergence Study has been defined as a standard on ASME V&V 20-2009 [21] and it is conducted in each test case for calibration.

The Grid Convergence Study is based on three different structured grids where the grid is being refined by a factor of $r = 1.45 - 1.5$ in each direction (Tab. 2). Therefore, the total cell count is increased by a factor of r^3 per refinement and the similarity to the basic grid is maintained, since no cell stretching can occur. Integral quantities such as the drag coefficient c_d are determined on each grid. This allows the extrapolation of a c_d value for an infinitely fine grid that does not exhibit any discretization errors. Based on this ideal c_d value, the resulting error on each grid can be estimated. In both test cases, the best trade-off between accuracy and feasibility was achieved with the medium fine grid.

5 MODEL FORMULATION

The $\gamma - Re_\theta$ -transition model provides two paths to influence the transition process. One path uses the $\tilde{Re}_{\theta t}$ transport equation and another path is to increase γ . The latter one is used by Watanabe et al. [11] and supports a rapid transition. The first one is used by Seyfert and Krumbein [9] for crossflow-induced transition, as well as by Herbst et al. [16] and Dassler et al. [22] for active flow control and roughness-induced transition. The prior described structure of the $\gamma - Re_\theta$ -model implies that modifying the $\tilde{Re}_{\theta t}$ equation provides an evolving destabilization of the boundary layer. As a result, flow historical effects can be taken into account. Each excess on $\tilde{Re}_{\theta t}$ introduces further disturbances into the boundary layer which sum up and finally initiate transition.

Table 2: Results of the Grid Convergence Study based on c_d

i	N	c_d	r	GCI	$EERE$
ONERA 'D'				$p = 2.132$	
$f_{c,3}$	$1.24 \cdot 10^6$	0.054479	-	0.0452	0.0356
$f_{c,2}$	$3.78 \cdot 10^6$	0.055579	1.45	0.0205	0.0161
$f_{c,1}$	$12.85 \cdot 10^6$	0.056108	1.5	0.0085	0.0068
$f_{e,p=2.132}$	∞	0.0565			
NLF(2)-0415				$p = 1.86$	
$f_{c,3}$	$0.96 \cdot 10^6$	0.0835	-	0.2351	0.1723
$f_{c,2}$	$3.06 \cdot 10^6$	0.0925	1.47	0.1142	0.0837
$f_{c,1}$	$10.5 \cdot 10^6$	0.097	1.5	0.0507	0.039
$f_{e,p=1.86}$	∞	1.009			

As observed by Arnal and Casalis [3], instabilities may be induced into the boundary layer by crossflow vortices, which trigger the development of Tollmien-Schlichting waves further downstream. This physical relationship can be realized by using $\tilde{Re}_{\theta t}$ to destabilize the boundary layer in case a crossflow is present. This persisting disturbance makes the boundary layer prone to further destabilization. Therefore, $\tilde{Re}_{\theta t}$ is utilized in the present model.

The transport equation

$$\frac{\partial(\rho\tilde{Re}_{\theta t})}{\partial t} + \frac{\partial(\rho U_j \tilde{Re}_{\theta t})}{\partial x_j} = P_{\theta t} + \frac{\partial}{\partial x_j} \left[\sigma_{\theta t} (\mu + \mu_t) \frac{\partial \tilde{Re}_{\theta t}}{\partial x_j} \right] \quad (2)$$

for the Reynolds number based on the momentum thickness is modified by the production term

$$P_{\theta t} = c_{\theta t} \frac{\rho}{t} (Re_{\theta t} - \tilde{Re}_{\theta t}) (1.0 - F_{\theta t}), \quad (3)$$

where $Re_{\theta t}$ is the local Reynolds number and $\tilde{Re}_{\theta t}$ is the transport quantity. $Re_{\theta t}$ is correlated to the findings of Abu-Ghannam and Shaw [14], therefore it considers the effects of the streamwise velocity gradient as well as the grade of turbulence.

The production term $P_{\theta t}$ is used to modify $\tilde{Re}_{\theta t}$ so that it is equal to $Re_{\theta t}$ outside of the boundary layer. In order to blend in $P_{\theta t}$ the function $F_{\theta t}$ is introduced. Within the boundary layer $F_{\theta t} = 1.0$ and outside the boundary layer it is set to $F_{\theta t} = 0$. By means of diffusion, $\tilde{Re}_{\theta t}$ is finally transported into the boundary layer, where it interacts with γ .

In the present crossflow model an additional production term

$$P_{CF} = - \min \left(\max \left[0, \left(\frac{\rho}{1000 \cdot t} \cdot \left(\frac{Re_H}{6} \right)^{c_1} \cdot \left(Re_{\Omega} \right)^{c_2} \cdot \left(\frac{12 \theta}{y} \right)^{c_3} - c_4 \right) \cdot c_5 \right], c_6 \right) \quad (4)$$

is added to Eq. 2. P_{CF} is always negative, since lowering $\tilde{Re}_{\theta t}$ is triggering transition. This production term is the key part of the present crossflow model. It consists of three terms which quantify the intensity of the crossflow and therefore the resulting disturbance of the boundary layer. Each of the terms is weighted by the exponent c_1 to c_3 .

The first and most important term is the Reynolds number based on the momentum thickness as well as the local helicity

$$Re_H = \frac{\theta}{\nu} \sqrt{\theta H}. \quad (5)$$

The focus is set on the helicity

$$H = \left| u_i \cdot \omega_i \right| \quad (6)$$

which is the magnitude of the scalar product of the velocity u_i and the vorticity ω_i . Therefore, it is maximized if the flow is rotating around the velocity vector. This is exactly what is observed in the area of crossflow instabilities in an accelerated boundary layer. The occurring vortices are aligned under a very low deflection angle assigned to the main flow vector [4, 3, 1]. This phenomenon is closely connected to those modelled by Herbst et al. [16] in the case of a jet in crossflow. As a result, the intensity of H is directly related to the sweep angle and the velocity. Additionally Reynolds dependencies are covered by integrating H into a formulation of a Reynolds number Re_H .

Another term is the vorticity Reynolds number

$$Re_\Omega = \frac{\rho y^2}{\mu} \Omega \quad (7)$$

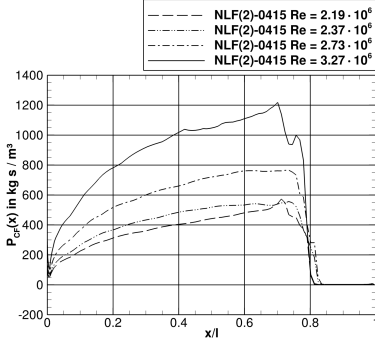
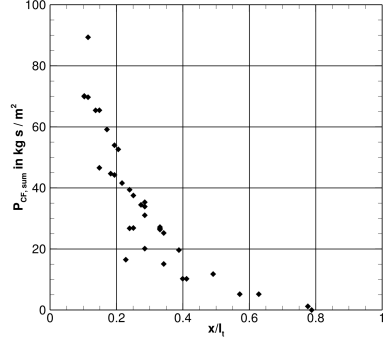
similar to the original formulation of Langtry and Menter [10], though it is rather based on the magnitude of the vorticity tensor Ω . This formulation goes along with the findings of Kato and Launder [19] who stated that $S \approx \Omega$ along most parts of the boundary layer, except the stagnation point where S exceeds Ω . As crossflow vortices start rising close downstream of the leading edge, the use of S would not be productive physically. It is therefore replaced by Ω . Re_Ω gives the ability to weight the influence of streamwise velocity components, independently from the crosswise velocity components.

The last term $\frac{\theta}{y}$ is used for correction. It was observed that Re_H based on θ operates well on a few test cases. On others, better results were obtained by the use of y instead. Therefore, $\frac{\theta}{y}$ was added to vary the two characteristic length scales independent from each other.

The crossflow model uses three additional constants c_4 to c_6 . c_4 is a limiter that has to be exceeded before the model starts to generate disturbances. The constant c_5 weights the overall destruction of $\tilde{Re}_{\theta t}$ and c_6 is used to border a maximum disturbance. The factor $\frac{\theta}{t}$ is added to maintain the same dimensions of $\tilde{Re}_{\theta t}$ in Eq. (2) and (3). Additional factors are included to raise all terms in Eq. (4) to an equal level.

6 MODEL CALIBRATION

Since the model is based on six calibration constants, which are linked in a complex manner, the calibration of this model is particularly challenging. In order to face up this task, an environment was created that allows an automated evaluation and presentation


Figure 2: Chordwise distribution of P_{CF}

Figure 3: Integral values of P_{CF} on the NLF(2)-0415; $Re = 3.27 \cdot 10^6$

of the calibration results. Furthermore new sets of calibration constants are suggested and a new generation of simulations is set up in a continuous loop.

The definition of new constants is based on an estimation function. To this end the maximum values of the parameters within the boundary layer, such as $Re_H(x)$, are plotted against the chord length. This allows the definition of a production term $P_{CF}(x)$ (Eq. 4 and Fig. 2) along the chord and furthermore to estimate the overall produced disturbances from the leading edge to the transition point by means of

$$P_{CF,sum} = \int_{x=0}^{x_t} w(x) P_{CF}(x) dx. \quad (8)$$

The weighting function $w(x)$ reflects the local receptivity of the boundary layer. It will not be discussed in this context. In Fig. 3 the link between the estimated $P_{CF,sum}$ and the transition positions, resulting from the CFD, are plotted. This basic idea is followed to define a new set of constants in an inverse procedure. As a result, only a few CFD calculations have to be performed in comparison to the broad series of constant sets that are evaluated.

7 RESULTS

Based on the calibration environment described in the previous section (Sec. 6), a set of calibration constants was defined that suits for all test cases. As presented in Fig. 4, the crossflow model can show a great dependency on the sweep angle and the Reynolds number. This strong dependency cannot be observed on the baseline $\gamma - Re_\theta$ -model. The observed results closely follow the experimental data and therefore underline the great potential of the investigated approach. The set of constants underlines the strong

$$\begin{aligned} c_1 &= 0.548 & c_2 &= 0.1912 & c_3 &= -0.298 \\ c_4 &= 0.0 & c_5 &= 60.0 & c_6 &= 1666.5 \end{aligned}$$

influence of the helicity Reynolds number Re_H that is the dominant factor since it is

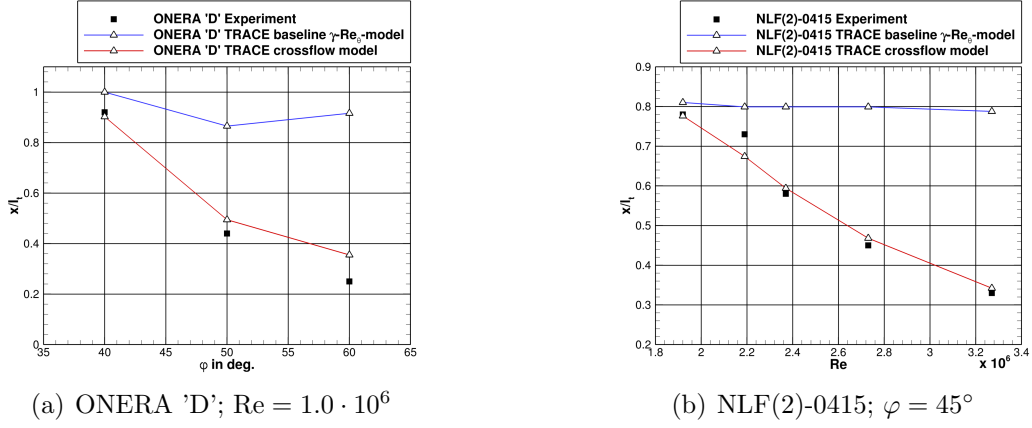


Figure 4: Comparison of the predicted and measured transition location

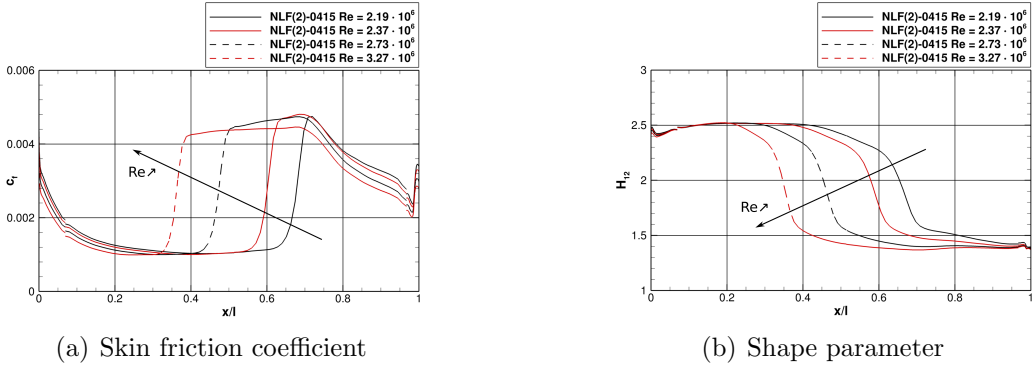


Figure 5: Quantitative evaluation of the transition location

weighted with the exponent $c_1 > c_2 > c_3$. The constant c_3 turns out to be negative. This follows the expectations described in Sec. 5. $(\frac{\theta}{y})^{c_3}$ makes y more influential.

The convergence of the simulation was ensured on all test cases except the ONERA 'D' profile at $\varphi = 60^\circ$. In this case, the transition position alternated strongly between $0.16 < x/l_t < 0.55$. The same tendency was observed when using the baseline $\gamma - Re_\theta$ -model, although in this case a delayed convergence was achieved. Therefore these convergence problems are not initiated but amplified by the crossflow model. The final transition location $x/l_t = 0.355$ was defined as the arithmetic mean of the maximum and minimum value.

In Fig. 5(a) the skin friction coefficient c_f and in Fig. 5(b) the boundary layer shape parameter H_{12} are plotted along the dimensionless chord. The skin friction shows a sharp rise, close to the transition point x/l_t . This is a clear indicator of a completed transition process. Similarly the shape parameter drops from $H_{12} \approx 2.59$ (suitable for a Blasius boundary layer) to $H_{12} \approx 1.4$, representing a turbulent boundary layer.

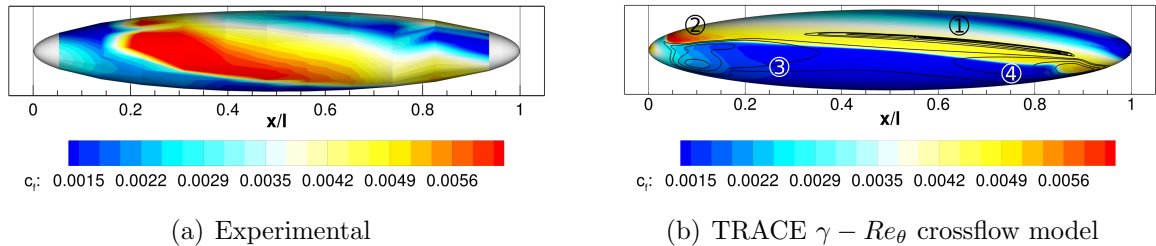


Figure 6: Comparison of the predicted and measured skin friction coefficient c_f along the 1:6 spheroid surface; contour lines indicate levels of Re_H ; $Re = 6.5 \cdot 10^6$; $\alpha = 15^\circ$

8 MODEL VALIDATION

The modified $\gamma - Re_\theta$ -model was validated on a 1:6 spheroid, which was experimentally investigated by Kreplin et al. [13]. The spheroid exhibits complex three-dimensional flow structures and therefore represents a challenging test case for transition models. In order to maximize the crossflow intensity, a setup with a high Reynolds number $Re = 6.5 \cdot 10^6$ and a high angle of attack $\alpha = 15^\circ$ was chosen. The level of turbulence is set to $Tu = 0.1\%$ at the spheroid tip.

When numerical and experimental results were compared in terms of the skin friction c_f (Fig. 6), a high grade of compliance was observed at the upper part of the spheroid ①. Close to position ②, a peak value of c_f was predicted at $x/l = 0.05$ while an equivalent peak was measured at $x/l = 0.2$. The major discrepancy was found at the lower part close to the position ③. The authors assume that this might be the result of an excessive stabilization of the accelerated boundary layer. Since high levels of Re_H are indicated by contour lines the model does detect the present crossflow but is not able to overcome the high grade of stabilization. These elevated Re_H levels can be found at position ④ correlating with a sharp rise of c_f close to $x/l = 0.85$ in the experimental data. As a result the authors want to state, that the fundamental behaviour of the crossflow model corresponds to the flow physics, however there is still a demand of more considerable modelling on this test case.

9 CONCLUSIONS

In the present paper, an extension of the $\gamma - Re_\theta$ -model is presented. This allows the prediction of crossflow-induced transition on swept-wing flows. The fundamental parameter of this transition model is Re_H , the Reynolds number based on the local helicity. It turned out that Re_H is a useful and reliable parameter for the detection of crossflows.

The model was calibrated by using an individually designed environment that is able to preliminary estimate the fitness of a set of calibration constants, followed by a suggestion of an improved constant set.

As the model is based on six constants, it was possible to calibrate it highly accurately

on two different experimentally investigated test cases of infinite swept-back wings. In each of these test cases, either the Reynolds number or the sweep angle, were varied. Therefore, major effects leading to crossflow instabilities can be captured by this model.

Since the model formulation is based on local variables, it can predict transition on complex three-dimensional geometries. The ability of the Re_H parameter was proven on the spheroid investigated by Kreplin et al. [13], however more intensive model access at high Reynolds numbers is obviously required. In the future, the segmental swept wing introduced by Petzold and Radespiel [8] will be an appropriate validation test case.

REFERENCES

- [1] Saric, W. S., Reed, H. L., and White, E. B., 2003. “Stability and transition of three-dimensional boundary layers”. *Annual Review of Fluid Mechanics*(35), pp. 413–440.
- [2] Dagenhart, J., and Saric, W., 1999. “Crossflow stability and transition experiments in swept-wing flow”. *NASA Langley Technical Report Server*(NASA/TP-1999-209344).
- [3] Arnal, D., and Casalis, G., 2000. “Laminar-turbulent transition prediction in three-dimensional flows”. *Progress in Aerospace Sciences*(36), pp. 173–191.
- [4] Poll, D. I. A., 1985. “Some observations of the transition process on the windward face of a long yawed cylinder”. *Journal of Fluid Mechanics*(150), pp. 329–356.
- [5] Kohama, Y., 1987. “Some expectation on the mechanism of cross-flow instability in a swept wing flow”. *Acta Mechanica*(66), pp. 21–38.
- [6] Deyhle, H., and Bippes, H., 1996. “Disturbance growth in an unstable three-dimensional boundary layer and its dependence on environmental conditions”. *Journal of Fluid Mechanics*, **316**, pp. 73–113.
- [7] Mayle, R. E., 1991. “The role of laminar-turbulent transition in gas turbine engines”. *Journal of Turbomachinery*, **113**(4), pp. 509–536.
- [8] Petzold, R., and Radespiel, R., 2013. “Transition on a wing with spanwise varying crossflow evaluated with linear stability theory”. *Fluid Dynamics Conference*, **43**(AIAA 2013-2466).
- [9] Seyfert, C., and Krumbein, A., 2012. “Correlation-based transition transport modeling for three-dimensional aerodynamic configurations”. *AIAA Aerospace Science Meeting*, **50**(AIAA 2012-0448).
- [10] Langtry, R. B., and Menter, F. R., 2009. “Correlation-based transition modeling for unstructured parallelized computational fluid dynamics codes”. *AIAA Journal*, **47**(12), pp. 2894–2906.

- [11] Watanabe, Y., Misaka, T., and Obayashi, S., 2009. “Appliction of crossflow transition criteria to local correlation-based transition model”. *AIAA Aerospace Science Meeting*, **47**(AIAA 2009-1145).
- [12] Kohama, Y., and Davis, S., 1993. “A new parameter for predicting crossflow instability”. *JSME International Journal*, **36**(1), pp. 80–85.
- [13] Kreplin, H.-P., Vollmers, H., and Meier, H. U., 1985. “Wall shear stress measurements on an inclined prolate spheroid in the DFVLR 3m x 3m low speed wind tunnel, Göttingen”. *DFVLR-AVA, report IB 22-84 A33*.
- [14] Abu-Ghannam, B. J., and Shaw, R., 1980. “Natural Transition of Boundary Layers—the Effects of Turbulence, Pressure Gradient, and Flow History”. *Journal of Mechanical Engineering Sciences*, **22**, pp. 213–228.
- [15] Nürnberger, D., Eulitz, F., Schmitt, S., and Zachcial, A., 2001. “Recent progress in the numerical simulation of unsteady viscous multistage turbomachinery flow”. *International Symposium on Air Breathing Engines*(1081).
- [16] Herbst, F., Fiala, A., and Seume, J. R., 2014. “Modeling vortex generating jet-induced transition in low-pressure turbines”. *Journal of Turbomachinery*, **136**(DOI:10.1115/1.4025735).
- [17] Roe, P. L., 1981. “Approximate riemann solvers, parameter vectors, and difference schemes”. *Journal of Computational Physics*(43), pp. 357–372.
- [18] Wilcox, D. C., 1988. “Reassessment of the scale-determining equation for advanced turbulence models”. *AIAA Journal*, **26**(11), pp. 1299–1309.
- [19] Kato, M., and Launder, B. E., 1993. “The modelling of turbulent flow around stationary and vibrating square cylinders”. *9th Symposium on Turbulent Shear Flows*, **1**, pp. 10.4.1–10.4.6.
- [20] Schmitt, V., and Manie, F., 1979. “Écoulements subsoniques et transsoniques sur une aile a flèche variable”. *Le Recherche Aérospatiale*(4), pp. 219–237.
- [21] ASME V & V 20 Committee, 2009. “Standard for verification and validation in computational fluid dynamics and heat transfer”. *The American Society of Mechanical Engineers*, pp. 213–228.
- [22] Dassler, P., Kožulović, D., and Fiala, A., 2012. “An approach for modelling the roughness-induced boundary-layer transition unusing transport equations”. *European Congress on Computational Methods in applied Science and Engineering (ECCOMAS 2012)*.